CLOUD MASK FOR CERES FROM VIRS ON THE TRMM SATELLITE

P. Minnis, D. F. Young
Atmospheric Sciences Division
NASA Langley Research Center
Hampton, Virginia, USA

D. A. Spangenberg, P. W. Heck, D. R. Doelling
AS&M, Inc.
Hampton, Virginia USA

Q. Trepte, Y. Chen
Science Applications International Corporation
Hampton, Virginia, USA

Proceedings of ALPS 99 Symposium
Meribel, France
18-22 January 1999
WK-P-06, pp. 1,4

CLOUD MASK FOR CERES FROM VIRS ON THE TRMM SATELLITE

Minnis, Patrick and Young, David F.
Atmospheric Sciences Division, NASA Langley Research Center, Hampton, VA 23681 USA

Spangenberg, Douglas A.; Heck, Patrick W.; Doelling, D. R.
AS&M, Inc., Hampton, VA 23666 USA

Trepte, Qing and Chen, Yan
Science Applications International Corporation, Hampton, VA 23666 USA

Introduction

Determination of cloud properties and the proper application of bidirectional reflectance models for computing top-of-the-atmosphere broadband fluxes from radiances first require accurate identification of the underlying scene. The Clouds and Earth's Radiant Energy System (CERES, see Wielicki et al., 1998) experiment on the 35°-inclined-orbit Tropical Rainfall Monitoring Mission (TRMM) satellite and on the upcoming Sun-synchronous EOS satellites is using two methods to categorize the type of scene in a given 25-km CERES footprint. The first technique is the maximum likelihood method (MLE) used by the Earth Radiation Budget Experiment (ERBE) and, later, by the ScaRaB project. Each footprint is classified as clear, partly cloudy, mostly cloudy, and overcast with subdivisions for land, water, coast, snow, and desert. These categories are used to select the anisotropic directional models to correct longwave and shortwave radiances to fluxes. The second technique uses the 2-km resolution TRMM Visible InfraRed Scanner (VIRS) which measures radiances in five channels: 0.65, 1.6, 3.75, 10.8, and 12.0 μm. The radiances are used to classify each imager pixel as clear or cloudy. The pixel values are then convolved to match the CERES broadband scanner field of view. The results of this technique can provide the same types of classifications as the MLE and, in conjunction with the derived cloud properties, a broader set of categories that account for cloud height, phase, particle size, and optical depth. This paper describes the current methodology for classifying each pixel of the VIRS dataset.

Basic Approach

The CERES cloud mask is basically a threshold method that defines a VIRS pixel as cloudy if one or more of its five radiances differs significantly from the expected clear-sky radiances. A cloudy pixel may be classified as strong or weak depending on how much the radiances differ from the predicted clear-sky radiances. Pixels identified as clear are designated as weak, strong, but may also be categorized as being filled with smoke, fire, or aerosol, contaminated by sunglint, or covered with snow. The daytime (solar zenith angle less than 78°) masking algorithm can utilize all five channels, while the nighttime technique can only employ channels 3, 4, and 5. To effect the scene classification, expected clear radiances and their uncertainties are required. Although the clear radiances are estimated differently for each channel, each radiance must be specified for a given latitude λ, longitude φ, time of day t, month m, solar zenith angle θ_o, viewing zenith angle θ, and relative azimuth angle Ψ. The clear-sky radiances are predicted at a 10' latitude-longitude resolution, but are sometimes only defined at the 1° level. Each 10' box is defined as water, permanent snow, or land and has a mean altitude $z_s(\lambda,\varphi)$ associated with it.

Visible Clear-sky Reflectance

The channel-1 (visible) clear-sky reflectance is

$$\rho_{cs1} = \alpha_1(\lambda,\varphi,m)\, \delta_1(\theta_o)\, \chi_1(\theta_o,\theta,\Psi), \qquad (1)$$

where α_1 is the overhead-sun albedo, δ_1 is the normalized directional reflectance model, and χ is the bidirectional distribution function. Except for ocean, the values of δ_1 are defined for each of 19 IGBP (International Geosphere Biosphere Programme; Belward and Loveland, 1996) surface types k from composites of clear ERBE scanner data taken between 1985 and 1990. The values of χ are from Minnis and Harrison (1984) for ocean and land and from Suttles et al. (1988) for desert and snow.

The clear-sky albedos and directional models for ocean are derived from an updated version of the clear ocean model of Minnis and Harrison (1984). The overhead-sun albedos for all other areas are derived using the 32-km resolution clear reflectances from the International Satellite Cloud Climatology Program (ISCCP) NOAA-9 Advanced Very High Resolution DX data taken during 1986 and 1987. The reflectances falling in a given 1° region are converted to α_1 using (1) and used to compute the mean and standard deviation for each pass during the month. The means for each region are then used to compute the average overhead albedo and its temporal standard deviation for the month. The relative rms average $\sigma_1(\lambda,\varphi,m)$ of the temporal and spatial standard deviations is normalized to $\langle\alpha_1\rangle$ to determine the basic uncertainty in a given value of $\langle\alpha_1\rangle$.

Mean values of $\alpha_1(k,m)$ and $\sigma_1(k,m)$ are then computed from the regions with data. The results for each month are filtered to eliminate poor sampling. All unfilled regions are then assigned the appropriate $\alpha_1(k,m)$ and $\sigma_1(k,m)$. In application, (1) is solved using the filled dataset. These clear 1° albedos are then used in an initial cloud-mask analysis of 1 month of 4-km resolution AVHRR data. If the 4-km clear-sky reflectances differ substantially from the DX results in a given 10' box, the albedo for the box is updated to reflect the high-resolution observations. The result is a much more realistic 10' overhead albedo for application to the VIRS data.

Near-infrared Reflectance

Because global measurements of 1.6-μm albedos are not readily available, they must be derived from the VIRS data using an initial pass through the dataset. The albedos are computed at surface level by first adjusting the top-of-atmosphere (TOA) reflectance through removal of the attenuation by the atmosphere (mainly by water vapor absorption) using the available vertical profiles of temperature and humidity. The channel-2 surface reflectance is

$$\rho_{s2} = \alpha_{s2}(\lambda,\varphi,m)\,\delta_2(\theta_o)\,\chi_2(\theta_o,\theta,\Psi), \qquad (2)$$

where the values of δ_2 and χ_2 are derived from aircraft data. The data are processed in the same manner as the visible albedos to develop monthly mean albedo and standard deviation maps at a 10' resolution.

Solar-infrared Clear-sky Temperature

The 3.7-μm radiance leaving the surface is approximated as

$$B_3(T_{s3}) = \varepsilon_3\{B_3(T_{skin})\} + \alpha_3\,\delta_3(\theta_o)\,\chi_3 S_3', \qquad (3)$$

where B_3 is the Planck function, T_{skin} is the surface skin temperature, ε_3 is the surface emissivity, T_{s3} is the apparent surface temperature at 3.7 μm, and S_3' is the solar radiation incident at the surface. $B_3(T_{s3})$ is then corrected for attenuation by the atmosphere to predict the clear-sky temperature T_{cs3}. The surface emissivities for channels 3, 4, and 5 are derived from the clear-sky ISCCP DX data using the method described by Minnis et al. (1998). Means and standard deviations are computed and all 1° regions are filled using the IGBP-type averages. The values are of δ_3 and χ_3 are specified using δ_1 and χ_1, respectively. This approach yields a mean difference between the observed and predicted values of T_{cs3} of –2 to +2K and –1 to +1K during daytime and nighttime, respectively, with standard deviations σ_3 less than 3K and 2K.

Infrared Temperatures

To estimate the 10.8-μm TOA temperature, interpolated 3- or 6-hourly skin temperatures computed by a high-resolution numerical weather analysis model are related to coincident ISCCP D1 clear-sky temperatures corrected to the surface level for each 2.5° region. A correction factor

$$\Delta T_{s4} = c_o + \sum_{i=1}^{2} c_i \sin \tfrac{it}{2\pi} + c_{i+2} \cos \tfrac{it}{2\pi} \qquad (4)$$

is then computed to bring the model temperature into agreement with the ISCCP-based value. When applied, the model skin temperature is adjusted with ΔT_{s4}, to give the apparent skin temperature T_{s4}. then attenuated to the TOA to yield the clear-sky temperature T_{cs4}. The estimated skin temperature is

$$T_{skin} = B_4^{-1}\{B_4(T_{s4}) / \varepsilon_4\}.$$

The uncertainties in the clear-sky temperatures are estimated as the standard deviations between the predicted and observed temperatures. A minimum of 2.5 K is set for ocean and 3.0K for land.

The apparent channel-5 (12 μm) skin temperature then is

$$T_{s5} = B_5^{-1}[\varepsilon_5\{B_5(T_{skin})\}].$$

It is adjusted to the TOA to produce T_{cs5}. The uncertainties in T_{cs5} are estimated to be the same as those for channel 4.

Daytime Mask

Each pixel is classified during daylight using a sequence of tests as outlined in Fig. 1. The first or "A" test screens out all pixels that are obviously too cold to be cloudfree. If $T_4 < T_A$, then the pixel is considered strongly cloudy. The value of T_A is equal to the temperature at 500 mb over land or to T_{skin} – 20K over ocean. If the pixel is not cloudy after (fails) the A test, it is then tested against the expected clear-sky

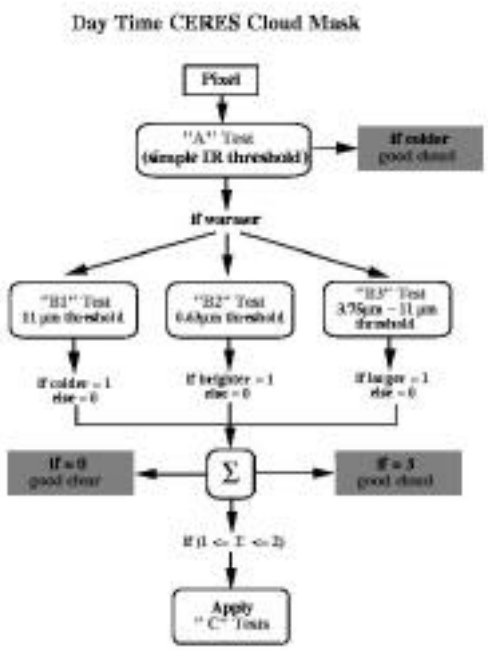

Fig. 1. Daytime CERES cloud mask algorithm.

radiances in the "B" tests, in which the parameters B1, B2, and B3 are initialized to 0.

1) If $T_4 < T_{cs4} - \sigma_4$, B1 = 1.

2) If $\rho_1 > \rho_{cs1}\,(1 + \sigma_1)$, B2 = 1.

3) If $T_3 - T_4 > T_{cs3} - T_{cs4} + \sigma_3$, B3 = 1.

If the sum of these parameters is 0 or 1, then the pixel is either good clear or cloudy, respectively. Otherwise, a more complicated set of "C" tests are then applied depending on the B tests that failed and the surface type. The C tests adjust the uncertainties and may involve channels2 or 5. From these C tests, a pixel categorized as clear may be assigned additional classifiers such as good, weak, aerosol, smoke, fire, or glint. Cloudy pixels may be classified as good, weak, glint, or multilayered.

Nighttime Mask

The nighttime mask follows a similar approach as seen in Fig. 2.. The A test, which is the same as the daytime A test is followed by 'D' tests that begin with D1 = D2 = D3 = 0.

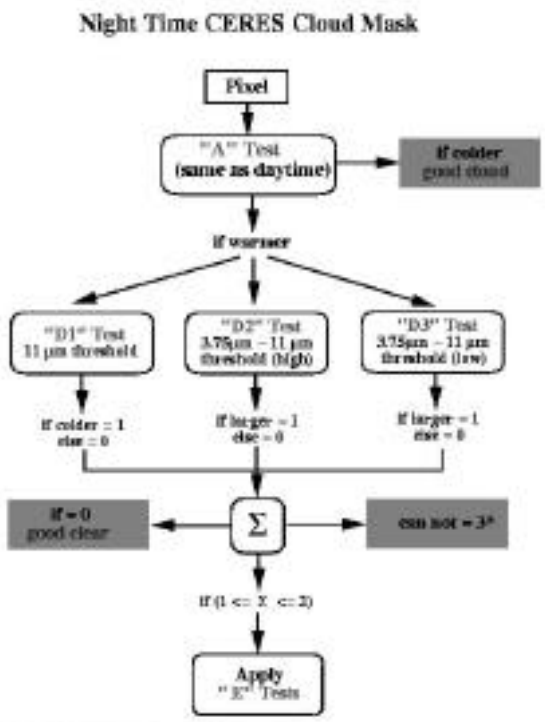

Fig. 2. CERES nighttime cloud mask algorithm.

The D1 and D2 tests are the same as B1 and B2, respectively. The D3 test checks determine if $T_3 - T_4 < T_{cs3} - T_{cs4} - \sigma_3$. If any of the D tests passes, then more complex E tests are applied that involve refined thresholds and channel 5. Otherwise, the pixel is classified as clear. The E tests will yield good or weak clear or good or weak cloudy classifications.

Results

The masks have been applied to VIRS version-1 data taken during January 1998 between 38°S and 38°N. During daytime, the A test classified 17% of the pixels as cloudy, while the B tests determined whether another 59% of the data were clear or cloudy. The C tests categorized the remaining 29%. At night, the A test found 16% of the pixels were cloudy, while the D tests found that 26% were clear. The E tests classified the remaining 58%.

From these results, the mean daytime cloud fraction was 57.3% compared to 55.1% for the nighttime. Of the daytime cloudy pixels, 6% were classified as weak and 4% as glint-affected clouds. The clear pixels were less certain; 8% were weak and 11% were contaminated by sunglint. Out of the clear land pixels, 4.5% were snow covered, 0.3% smoke filled, and 0.1% were affected by fires. At night, 30% of the cloudy pixels were weak and 22% of the land pixels were weak.

Concluding Remarks

The CERES mask is still subject to further improvement as more clear-sky and bidirectional reflectance data become available. The initial results are quite reasonable and will aid the development of improved cloud anisotropic models and as a basis for understanding the relationship between cloud properties and the radiation budget.

References

Belward, A. and T. Loveland, 1996: The DIS 1km land cover data set. In *Global Change*, The IGBP Newsletter, #27, Sep., 1996 [Available from IGBP Secretariat]

Minnis, P. and E. F. Harrison, 1984: Diurnal variability of regional cloud and clear-sky radiative parameters derived from GOES data. Part III: November 1978 radiative parameters. *J. Climate Appl. Meteorol.*, **23**, 1032-1052.

Minnis, P., W. L. Smith, Jr., and D. F. Young, 1998: Surface emissivity derived from multispectral satellite data. *Proc. 8th Ann. ARM Science Team Mtg.*, Tuscon, AZ, March 23-27, 489-494.

Suttles, J. T., R. N. Green, P. Minnis, G. L. Smith, W. F. Staylor, B. A. Wielicki, I. J. Walker, D. F. Young, V. R. Taylor, and L. L. Stowe, 1988: Angular radiation models for Earth-atmosphere system: Volume I - shortwave radiation. *NASA RP 1184*, 144 p.

Wielicki, B. A., B. R. Barkstrom, B. A. Baum, T. P. Charlock, R. N. Green, D. P. Kratz, R. B. Lee, P. Minnis, G. L. Smith, D. F. Young, R. D. Cess, J. A. Coakley, Jr., D. A. H. Crommelynck, L. Donner, R. Kandel, M. D. King, A. J. Miller, V. Ramanathan, D. A. Randall, L. L. Stowe, and R. M Welch., 1998: Clouds and the Earth's Radiant Energy System (CERES): Algorithm overview. *IEEE Trans. Geosci. Remote Sens.*, **36**, 1127-1141.